

# Coverage Dependence of the Level Alignment for Methanol on $\text{TiO}_2(110)$

Annapaola Migani<sup>a,\*</sup>, Duncan J. Mowbray<sup>b,\*</sup>

<sup>a</sup>ICN2 - Institut Català de Nanociència i Nanotecnologia and CSIC - Consejo Superior de Investigaciones Científicas, ICN2 Building, Campus UAB, E-08193 Bellaterra (Barcelona), Spain

<sup>b</sup>Nano-Bio Spectroscopy Group and ETSF Scientific Development Center, Departamento de Física de Materiales, Universidad del País Vasco UPV/EHU and DIPC, E-20018 San Sebastián, Spain

## ARTICLE INFO

### Article history:

Submitted April 22, 2014

### Keywords:

Level alignment

HOMO

Wet electron level

Two photon photoemission

Ultraviolet photoemission spectroscopy

Photocatalysis

## ABSTRACT

Electronic level alignment at the interface between an adsorbed molecular layer and a semiconducting substrate determines the activity and efficiency of many photocatalytic materials. We perform  $G_0W_0$  calculations to determine the coverage dependence of the level alignment for a prototypical photocatalytic interface:  $\frac{1}{2}$  and 1 monolayer (ML) intact and dissociated  $\text{CH}_3\text{OH}$  on rutile  $\text{TiO}_2(110)$ . We find changes in the wavefunction's spatial distribution, and a consequent renormalization of the quasi-particle energy levels, as a function of  $\text{CH}_3\text{OH}$  coverage and dissociation. Our results suggest that the occupied molecular levels responsible for hole trapping are not those observed in the ultraviolet photoemission spectroscopy (UPS) spectrum. Rather, they are those of isolated  $\text{CH}_3\text{O}$  on the surface. We find the unoccupied molecular levels have either 2D character with weight above the surface at 1 ML coverage, or significant hybridization with the surface at  $\frac{1}{2}$  ML coverage. These results suggest the resonance observed in the two photon photoemission (2PP) spectrum arises from excitations to unoccupied "Wet electron" levels with 2D character.

## 1. Introduction

$\text{TiO}_2$  is one of the most technologically important photocatalytic materials [1, 2]. Since the first report in the early 1970s of photocatalytic  $\text{H}_2\text{O}$  splitting on  $\text{TiO}_2$  electrodes [3], this material has been extensively investigated experimentally [4]. This is primarily due to its application in molecular hydrogen ( $\text{H}_2$ ) energy technology [5, 6]. In 1980, photocatalyzed  $\text{H}_2$  generation was shown to be remarkably enhanced when sacrificial  $\text{CH}_3\text{OH}$ , a hole trap, was added to  $\text{H}_2\text{O}$  [7].

Since then, the photocatalytic chemistry of  $\text{CH}_3\text{OH}$  on  $\text{TiO}_2$  has attracted an increasing amount of attention. In particular, model surface science experiments have been conducted on the single crystal rutile  $\text{TiO}_2(110)$  surface, under ultrahigh vacuum (UHV) and controlled coverage conditions. Experimentalists have characterized the electronic structure using ultraviolet, X-ray, and two photon photoemission spectroscopy (UPS, XPS, and 2PP) [8–15], scanning tunnelling microscopy (STM) [14–17], and reaction products using temperature programmed desorption (TPD) [10, 18–22]. These experiments have shown that  $\text{CH}_3\text{OH}$  can be photocatalytically dissociated on  $\text{TiO}_2(110)$  to form  $\text{CH}_3\text{O}$  and surface OH species [14, 21], and selectively photooxidized to  $\text{CH}_2\text{O}$  [19] and  $\text{HCOOCH}_3$  [10, 20]. Moreover, the formation of  $\text{CH}_2\text{O}$  can be accompanied by the photocatalyzed production of  $\text{H}_2$  [22]. A similar photocatalytic dissociation of  $\text{H}_2\text{O}$  on  $\text{TiO}_2(110)$  has been recently reported [23], although with a much lower efficiency.

The mechanism for these reactions is still unclear and requires an accurate theoretical treatment. The reaction begins upon irradiating the  $\text{TiO}_2$  photocatalyst with UV light at energies exceeding the band gap. This leads to the formation of electron-hole pairs. To understand the reaction mechanism, it is necessary to study the interaction of the photogenerated electron-hole pairs with adsorbed  $\text{CH}_3\text{OH}$  and  $\text{H}_2\text{O}$ . In particular, the energy level alignment of the occupied O 2p surface and frontier molecular levels determines both the mechanism and activity of the photooxidation processes (e.g.,  $\text{CH}_2\text{O}$  or  $\text{HCOOCH}_3$  formation). On the other hand, the level alignment of the unoccupied Ti 3d surface and frontier molecular levels determines the mechanism and activity of the photoreduction process (e.g.,  $\text{H}_2$  formation).

The level alignment of  $\text{CH}_3\text{OH}$  on  $\text{TiO}_2(110)$  has been probed by UPS for the occupied levels [8], and 2PP for the unoccupied levels [11]. Based on quasiparticle (QP)  $G_0W_0$  calculations for one monolayer (ML) of  $\text{CH}_3\text{OH}$  on  $\text{TiO}_2(110)$ , we recently showed that the molecular structures measured in both UPS [8] and 2PP [11] experiments are predominantly intact  $\text{CH}_3\text{OH}$  [24]. For 1 ML  $\frac{1}{2}$ -dissociated  $\text{CH}_3\text{OH}$  layers, we found the highest occupied molecular orbitals (HOMO) of  $\text{CH}_3\text{OH}$  are nearer the valence band maximum (VBM). This more favorable HOMO alignment may explain why  $\text{CH}_3\text{O}$  is more photocatalytically active than  $\text{CH}_3\text{OH}$  [24].

However, these experiments may incorporate lower coverage domains. Here, we will probe how the molecular coverage can directly modify the type, spatial distribution, and QP energy of the HOMO for intact and dissociated  $\text{CH}_3\text{OH}$  on  $\text{TiO}_2(110)$ . These are predominantly non-bonding O 2p orbitals, with some C–H  $\sigma$  character. The HOMO of the dissociating  $\text{CH}_3\text{OH}$  ( $\text{HOMO}_\text{D}$ ) and the non-dissociating  $\text{CH}_3\text{OH}$

\*Corresponding authors. Address: ICN2 Building, Campus UAB, E-08193 Bellaterra, Tel.: +34 937 37 3605 (Annapaola Migani). Address: Centro Joxe Mari Korta, Avenida de Tolosa 72, E-20018 San Sebastián, Tel.: +34 943 01 8392 (Duncan J. Mowbray).

Email addresses: annapaola.migani@cin2.es (Annapaola Migani), duncan.mowbray@gmail.com (Duncan J. Mowbray)

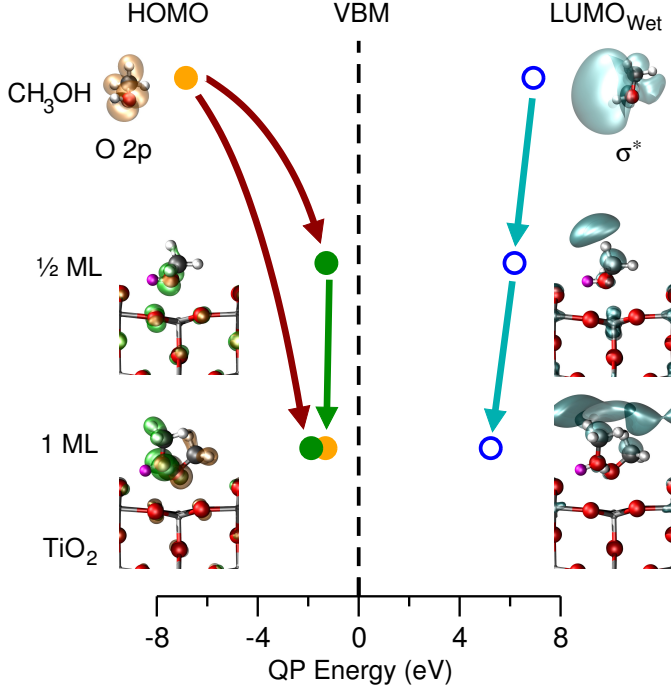


**Fig. 1.** Renormalization of the QP energies of HOMO and  $\text{LUMO}_{\text{Wet}}$  levels in the gas phase due to adsorption on  $\text{TiO}_2(110)$  for intact  $\text{CH}_3\text{OH}$   $1/2$  ML and 1 ML [24] coverages. H, C, O, Ti, and  $\text{H}^+$  atoms are represented by white, grey, red, silver, and magenta balls, respectively.

( $\text{HOMO}_{\text{ND}}$ ) are shown in Fig. 1 for  $\text{CH}_3\text{OH}$  in gas phase and  $1/2$  ML and 1 ML intact  $\text{CH}_3\text{OH}$  on  $\text{TiO}_2(110)$ .

In 2PP experiments of  $\text{CH}_3\text{OH}$  on  $\text{TiO}_2(110)$ , an excited resonance peak has been independently observed at about 2.4 eV [11, 12, 14, 15] above the Fermi level  $\varepsilon_F$ . This resonance is due to excitations from reduced  $\text{Ti}^{+3}$  3d levels located  $\sim 0.7$  eV below the Fermi level through an intermediate level to the vacuum using a 3.05 eV light source [12]. However, which intermediate electronic level is responsible for the observed 2PP resonance is still under debate.

On the one hand, H. Petek and coworkers [12] attribute the 2PP resonance to excitations through a “Wet electron” level. This electronic level has a two dimensional (2D)  $\sigma^*$  character associated with the  $\text{CH}_3\text{OH}$  C–H bonds, and significant weight above the H atoms outside the molecular layer [12, 24–26]. They report this resonance attains its maximum intensity at 1 ML coverage [11]. The lowest unoccupied molecular orbitals with Wet electron character ( $\text{LUMO}_{\text{Wet}}$ ) are shown in Fig. 1 for  $\text{CH}_3\text{OH}$  in gas phase and intact  $1/2$  ML and 1 ML coverages on  $\text{TiO}_2(110)$ .

On the other hand, X. Yang and coworkers [14, 15] attribute the 2PP resonance to the presence of dissociated  $\text{CH}_3\text{OH}$ , i.e.,  $\text{CH}_3\text{O}$ , on  $\text{TiO}_2(110)$ . Specifically, they state the 2PP resonance is from 3d levels of  $\text{CH}_3\text{O}$  occupied cus Ti sites. They find the 2PP resonance significantly increases in intensity and shifts to lower energy with illumination [14, 15]. For this reason, the 2PP resonance appears to be a consequence of  $\text{CH}_3\text{OH}$  pho-

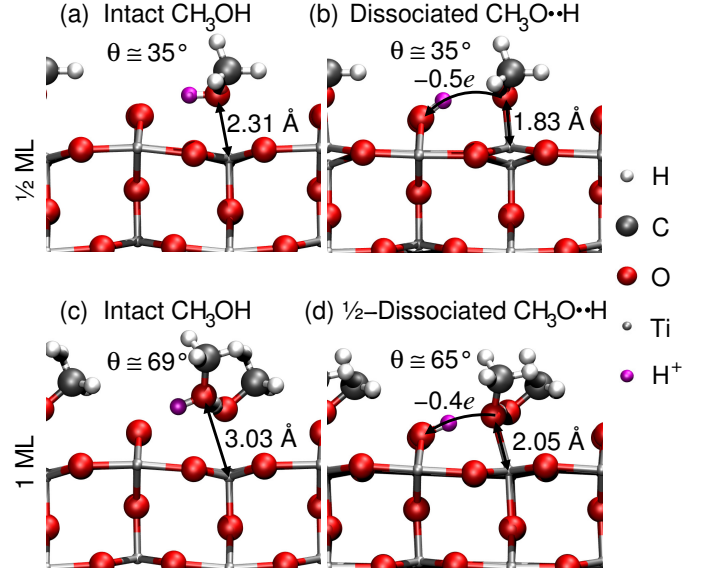


**Fig. 2.** The atomic structures of (a,b)  $1/2$  ML and (c,d) 1 ML [24, 26] of (a,c) intact, (b) dissociated, and (d)  $1/2$ -dissociated  $\text{CH}_3\text{OH}$  on  $\text{TiO}_2(110)$ . The transferred proton is marked in magenta, along with the accompanying charge transfer of (b) 0.5 and (d) 0.4 electrons. Relevant geometrical parameters of the dissociating  $\text{CH}_3\text{OH}$ , i.e. O–Ti distance in Å and molecular tilt  $\theta$  in  $^\circ$  relative to the surface, are also provided.

todissociation upon UV irradiation [14, 19]. Moreover, they report a similar resonance is observed at lower coverages ( $1/2$  ML and  $1/6$  ML).

At such low coverages, the  $\sigma^*$  levels of neighboring  $\text{CH}_3\text{OH}$  are not expected to interact. This means the Wet electron levels lose their 2D character, and should be destabilized. It is thus unclear whether a Wet electron level would be accessible at the 2PP resonance energy (2.4 eV) and lower coverages ( $1/2$  ML and  $1/6$  ML) [14, 19]. For this reason, X. Yang claims the 2PP resonance cannot be interpreted as a Wet electron level, as the latter is expected to be accessible only at higher coverages (1 ML) [14, 15].

Within the context of UPS and 2PP experiments, it is important to understand how the energy and spatial distribution of the  $\text{CH}_3\text{OH}$  HOMO and Wet electron levels change with the surface coverage and following dissociation. However, an accurate description of the interfacial level alignment requires a QP  $G_0W_0$  treatment. This is because the screening of the electron–electron interaction in photocatalytic interfacial systems has a strong spatial dependence [24, 25, 27–30]. In other words, interfacial levels are screened according to their weight in the bulk, molecular, and vacuum regions [24, 25].

In this paper, we perform  $G_0W_0$  calculations for the  $1/2$  ML intact and dissociated and the 1 ML intact and  $1/2$ -dissociated  $\text{CH}_3\text{OH}$  on  $\text{TiO}_2(110)$  structures shown in Fig. 2. 1 ML coverage corresponds to the adsorption of one  $\text{CH}_3\text{OH}$  per coordinately unsaturated (cus) Ti site, while  $1/2$  ML coverage corresponds to one  $\text{CH}_3\text{OH}$  for every other cus Ti site of the  $\text{TiO}_2(110)$  surface. In so doing, we show how the HOMO and

LUMO<sub>Wet</sub> CH<sub>3</sub>OH QP energies are renormalized upon absorption and increasing coverage on TiO<sub>2</sub>(110) (*cf.* Fig. 1).

## 2. Computational methods

The QP  $G_0W_0$  approach involves the single-shot correction of the Kohn-Sham (KS) density functional theory (DFT) eigenvalues by the self energy  $\Sigma = iGW$ , where  $G$  is the Green's function and  $W$  is the screening [31].  $W$  is obtained from the dielectric function, based on the KS wavefunctions [32]. This is calculated using linear response time-dependent DFT within the random phase approximation (RPA), including local field effects [33]. Through the  $G_0W_0$  technique one obtains a first-order approximation to the QP eigenvalues. However, the vacuum level  $E_{vac}$  and wavefunctions used are those from standard DFT.

All calculations have been performed using the DFT code VASP within the projector augmented wave (PAW) scheme [34]. We used a generalized gradient approximation (PBE) [35] for the xc-functional [36]. The geometries have been fully relaxed, with all forces  $\leq 0.02$  eV/Å, a plane-wave energy cutoff of 445 eV, an electronic temperature  $k_B T \approx 0.2$  eV with all energies extrapolated to  $T \rightarrow 0$  K, and a PAW pseudopotential for Ti which includes the  $3s^2$  and  $3p^6$  semi-core levels [37, 38].

We have modelled the atomic structures of  $1/2$  ML intact CH<sub>3</sub>OH and its dissociated counterpart on TiO<sub>2</sub>(110), as shown in Fig. 2(a) and (b). For the 1 ML coverage we have used the most stable structure of intact CH<sub>3</sub>OH and its  $1/2$ -dissociated counterpart on TiO<sub>2</sub>(110) [26] shown in Fig. 2(c) and (d). In each case we have included adsorbates on both sides of a four layer slab, with  $C_2$  symmetry. We used a  $1 \times 2$  unit cell of  $6.497 \times 5.916 \times 47.0$  Å<sup>3</sup>, corresponding to the experimental lattice parameters for bulk rutile TiO<sub>2</sub> [39] in the surface plane. This provides  $\geq 27$  Å of vacuum between repeated images.

We employed a  $\Gamma$  centered  $4 \times 4 \times 1$   $\mathbf{k}$ -point mesh, with 760 bands for  $1/2$  ML and 880 bands for 1 ML coverages, i.e.  $\sim 9.2$  unoccupied bands per atom, an energy cutoff of 80 eV for the number of  $\mathbf{G}$ -vectors, and a sampling of 80 frequency points for the dielectric function. We have previously shown that these parameters provide an accurate description of the level alignment for 1 ML of CH<sub>3</sub>OH on TiO<sub>2</sub>(110) [24] and the bulk rutile TiO<sub>2</sub> electronic band gap and optical spectrum [25].

The alignment of the experimental UPS and 2PP spectra for CH<sub>3</sub>OH on TiO<sub>2</sub>(110) has been performed relative to the VBM. This is accomplished by shifting by +3.2 eV the UPS and 2PP spectra, which are measured relative to the Fermi level. A more detailed discussion of the experimental energy references is provided in Ref. 25.

## 3. Results and discussion

We have performed  $G_0W_0$  QP calculations for the structures shown in Fig. 2. These correspond to  $1/2$  ML (intact and dissociated) and 1 ML (intact and  $1/2$ -dissociated) of CH<sub>3</sub>OH on TiO<sub>2</sub>(110).

For the  $1/2$  ML structures (a,b) CH<sub>3</sub>OH is adsorbed at the cus Ti site of the TiO<sub>2</sub>(110) surface. For the intact structure,

CH<sub>3</sub>OH forms an interfacial hydrogen bond with a neighboring bridging O atom ( $O_{br}$ ) of the surface. For the dissociated structure, CH<sub>3</sub>OH transfers a proton and an accompanying charge of 0.5 electrons to the  $O_{br}$ .

The 1 ML structures (c,d) have an additional CH<sub>3</sub>OH at an adjacent cus Ti site. This non-dissociating CH<sub>3</sub>OH forms an intermolecular hydrogen bond with the dissociating CH<sub>3</sub>OH. This additional coordination of the dissociating CH<sub>3</sub>OH raises it off the surface by about 0.7 Å, increases its tilt  $\theta$  by about 30°, and results in a reduction of the charge transferred to the  $O_{br}$  by about 0.1e upon dissociation, as shown in Fig. 2(c) and (d). Our aim is to see how these structural and electronic changes with coverage impact the interfacial level alignment of CH<sub>3</sub>OH on TiO<sub>2</sub>(110).

We begin by comparing the coverage dependence of the relevant interfacial molecular levels' spatial distribution. Specifically, in Fig. 3 we compare the isosurfaces and height dependence of the wavefunction densities for LUMO<sub>Wet</sub>, LUMO<sub>Wet</sub>+1, HOMO<sub>D</sub>, and HOMO<sub>ND</sub> for  $1/2$  ML (intact and dissociated) and 1 ML (intact and  $1/2$ -dissociated) of CH<sub>3</sub>OH on TiO<sub>2</sub>(110).

LUMO<sub>Wet</sub> for  $1/2$  ML structures (Fig. 3(a,c)) is more hybridized with the unoccupied surface Ti 3d levels compared to the 1 ML structures (Fig. 3(b,d)). Further, LUMO<sub>Wet</sub> for the dissociated  $1/2$  ML also overlaps with the  $O_{br}H$   $\sigma^*$  level. For the 1 ML there is sufficient coverage for LUMO<sub>Wet</sub> to have 2D character (*cf.* insets Fig. 3(b,d)). However,  $1/2$  ML coverage is insufficient for LUMO<sub>Wet</sub> to be 2D (*cf.* insets Fig. 3(a,c)). Finally, LUMO<sub>Wet</sub>+1 for the  $1/2$ -dissociated 1 ML lacks 2D character and is substantially hybridized with the surface Ti 3d levels, as we saw for the  $1/2$  ML LUMO<sub>Wet</sub>.

For the  $1/2$  ML intact structure (Fig. 3(a)), HOMO<sub>D</sub> is substantially hybridized with the O 2p <sub>$\pi$</sub>  levels [40] of the surface. For the 1 ML intact structure (Fig. 3(b)), HOMO<sub>D</sub> is mostly localized on CH<sub>3</sub>OH, while HOMO<sub>ND</sub> is somewhat more hybridized with the surface. The increased localization for 1 ML is consistent with the larger separation from the surface of the dissociating CH<sub>3</sub>OH shown in Fig. 2(c). In contrast, the reduced tilt for  $1/2$  ML of CH<sub>3</sub>OH (Fig. 2(a)) results in a stronger overlap with the O 2p <sub>$\pi$</sub>  levels of the three-fold-coordinated O atom ( $O_{3c}$ ) of the surface.

After dissociation, the HOMO<sub>D</sub> is more hybridized with the surface for both  $1/2$  ML and 1 ML coverages (Fig. 3(c,d)). The HOMO<sub>D</sub> O 2p lone pairs are similarly oriented for both 1 ML structures. However, the HOMO<sub>D</sub> O 2p lone pairs for the  $1/2$  ML intact and dissociated structures are oriented differently. After O–H bond dissociation, the O 2p orbital, which was previously involved in the O–H bond, becomes the least stable CH<sub>3</sub>OH O 2p lone pair, i.e., HOMO<sub>D</sub>.

Table 1 lists the LUMO<sub>Wet</sub>, LUMO<sub>Wet</sub>+1, HOMO<sub>D</sub>, and HOMO<sub>ND</sub> energy at  $\Gamma$  for  $1/2$  ML and 1 ML of CH<sub>3</sub>OH on TiO<sub>2</sub>(110).

For the 1 ML intact structure, the non-dissociating CH<sub>3</sub>OH pushes the dissociating molecule off the surface via steric hindrance. At the same time, their intermolecular H-bond prevents the dissociating CH<sub>3</sub>OH from desorbing. This stabilizes HOMO<sub>D</sub> relative to HOMO<sub>ND</sub> (Table 1). As a result, the

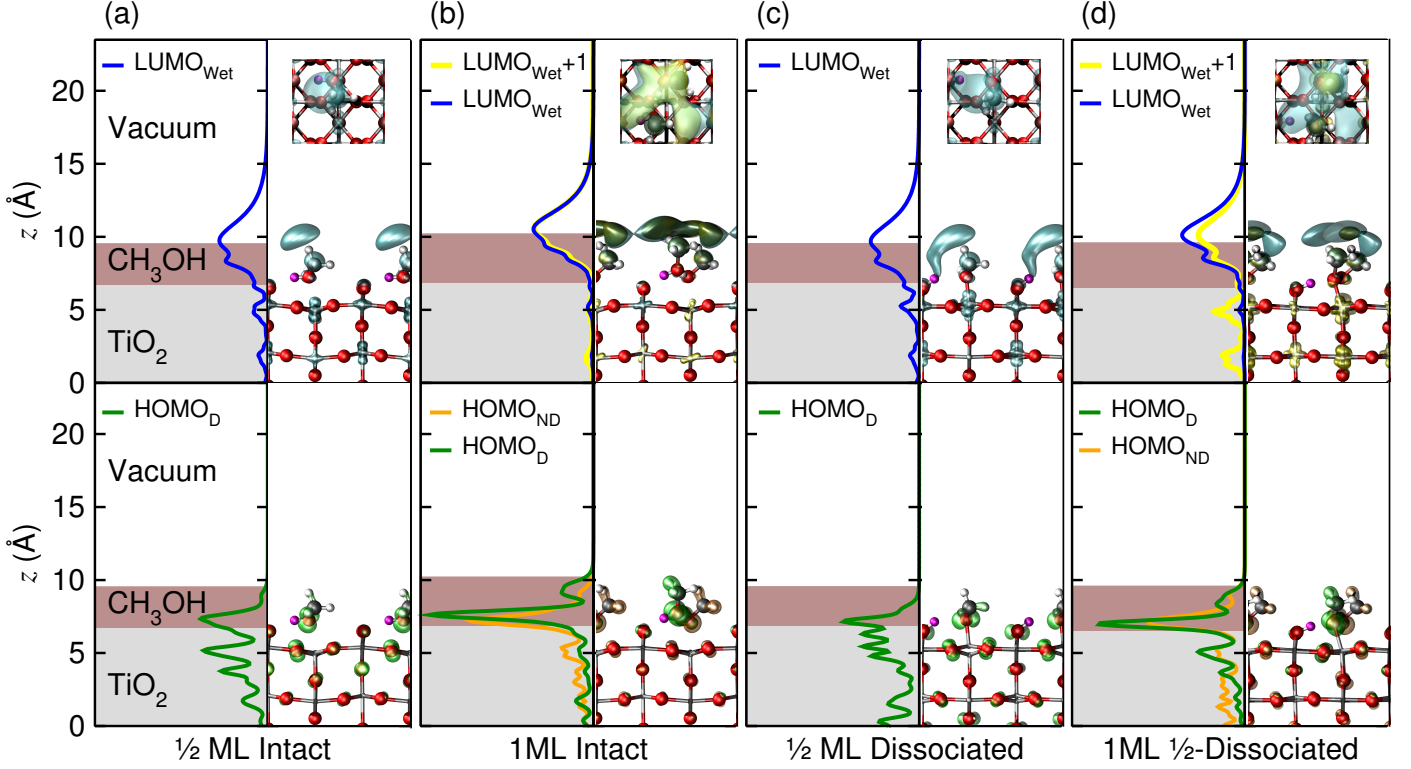


**Fig. 3.** Calculated  $\text{LUMO}_{\text{Wet}}$  (blue),  $\text{LUMO}_{\text{Wet}} + 1$  (yellow),  $\text{HOMO}_{\text{D}}$  for the dissociating  $\text{CH}_3\text{OH}$  (green), and  $\text{HOMO}_{\text{ND}}$  for the non-dissociating  $\text{CH}_3\text{OH}$  (orange) isosurfaces and their average densities in the  $xy$ -plane at  $\Gamma$  versus distance  $z$  in Å from the center of the  $\text{TiO}_2$  substrate for (a,b) intact, (c) dissociated, and (d)  $1/2$ -dissociated (a,c)  $1/2$  ML and (b,d) 1 ML [24]  $\text{CH}_3\text{OH}$  on  $\text{TiO}_2(110)$ .  $\text{TiO}_2$  bulk,  $\text{CH}_3\text{OH}$  molecular layer, and vacuum are depicted by grey, brown, and white regions, respectively. H, C, O, Ti, and  $\text{H}^+$  atoms are represented by white, grey, red, silver, and magenta balls, respectively.

$\text{HOMO}_{\text{D}}$  energy is closer to that of the isolated  $\text{CH}_3\text{OH}$  (Fig. 1). On the other hand, in the absence of this coordinating  $\text{CH}_3\text{OH}$ , the  $\text{HOMO}_{\text{D}}$  energy is close to the 1 ML  $\text{HOMO}_{\text{ND}}$  energy.

After dissociation,  $\text{HOMO}_{\text{D}}$  and  $\text{HOMO}_{\text{ND}}$  are shifted up to basically the same energy. This may be understood in terms of an increased interaction of the dissociated  $\text{CH}_3\text{OH}$  with the surface (*cf.* Fig. 3(d)).

Overall, the unoccupied  $\text{CH}_3\text{OH}$  levels may be classified into two groups based on their energies (Table 1) and spatial distribution (Fig. 3). The first group of levels is at lower energy (5.2–5.4 eV) and has a strong 2D character above the surface. This group consists of the intact 1 ML  $\text{LUMO}_{\text{Wet}}$  and  $\text{LUMO}_{\text{Wet}} + 1$  and the  $1/2$ -dissociated 1 ML  $\text{LUMO}_{\text{Wet}}$  levels. The second group of levels is at higher energy (6.0–6.2 eV), lacks 2D character, and is instead significantly hybridized with Ti 3d levels. This group consists of the intact and dissociated  $1/2$  ML  $\text{LUMO}_{\text{Wet}}$  and the  $1/2$ -dissociated 1 ML  $\text{LUMO}_{\text{Wet}} + 1$  levels.

Based on the observed groupings, we find Wet electron levels with 2D character are more stable by about 0.8 eV, as compared to those which are instead hybridized with the surface. In particular, after dissociation the 1 ML  $\text{LUMO}_{\text{Wet}} + 1$  level loses its weight on the dissociated  $\text{CH}_3\text{OH}$ , and thus its 2D character. This level is then significantly destabilized, and resembles in both energy and spatial distribution  $\text{LUMO}_{\text{Wet}}$  for  $1/2$  ML cov-

erage.

Already at the DFT level, we find the unoccupied levels are significantly stabilized by increasing the coverage from  $1/2$  ML to 1 ML. Overall, the 1 ML intact structure has the most stable  $\text{LUMO}_{\text{Wet}}$  levels. However, differences in the spatial distribution of the 1 ML  $1/2$ -dissociated Wet electron levels are not reflected in their KS eigenenergies. Capturing such effects requires a QP treatment to describe the anisotropic screening.

Due to the differences in their spatial distribution, 2D and surface hybridized Wet electron levels of the 1 ML  $1/2$ -dissociated structure are screened differently, resulting in different QP energy shifts. On the one hand, the 2D  $\text{LUMO}_{\text{Wet}}$  QP energy approaches that of the 1 ML intact  $\text{LUMO}_{\text{Wet}}$  levels. On the other hand, the surface hybridized  $\text{LUMO}_{\text{Wet}} + 1$  QP energy approaches that of the  $1/2$  ML  $\text{LUMO}_{\text{Wet}}$  levels. We have previously shown that there exists an intimate relationship between QP energy shifts and the wavefunction's spatial distribution [24, 25].

As shown in Fig. 3, the Wet electron levels are delocalized within the molecular plane, with weight inside and above the molecular layer. This means they may be screened based on their density averaged over the  $xy$ -plane. Specifically, they may be identified as the unoccupied levels with more than half their weight between the bridging O atom of the surface and 5 Å above the top of the molecular layer. It is these levels which are



**Table 1**

DFT and  $G_0W_0$  energies for the  $\text{HOMO}_D$ ,  $\text{HOMO}_{ND}$ ,  $\text{LUMO}_{\text{Wet}}$  and  $\text{LUMO}_{\text{Wet}} + 1$  levels, highest/lowest peak energies  $\varepsilon_{\text{peak}}^{\text{PDOS/Wet}}$  relative to the VBM  $\varepsilon_{\text{VBM}}$  for the  $\text{CH}_3\text{OH}$  PDOS/Wet DOS, and differences  $\Delta\varepsilon^{\text{UPS/2PP}}$  from the UPS/2PP measurements in eV, for the  $\frac{1}{2}$  ML (intact and dissociated) and 1 ML (intact and  $\frac{1}{2}$ -dissociated)  $\text{CH}_3\text{OH}$  on  $\text{TiO}_2(110)$ .

Method	Coverage	Molecular Layer	$\text{HOMO}_D$ (eV)	$\text{HOMO}_{ND}$ (eV)	$\varepsilon_{\text{peak}}^{\text{PDOS}}$ (eV)	$\Delta\varepsilon^{\text{UPS}}$ (eV)	$\text{LUMO}_{\text{Wet}}$ (eV)	$\text{LUMO}_{\text{Wet}} + 1$ (eV)	$\varepsilon_{\text{peak}}^{\text{Wet}}$ (eV)	$\Delta\varepsilon^{\text{2PP}}$ (eV)
DFT	$\frac{1}{2}$ ML	Intact	-0.83	—	-0.88	+0.67	+5.51	—	+5.73	+0.15
	1 ML	Intact	-0.85	-0.61	-0.76 <sup>a</sup>	+0.79 <sup>a</sup>	+4.61	+4.62	+4.96 <sup>a</sup>	-0.62 <sup>a</sup>
	$\frac{1}{2}$ ML	Dissociated	-0.43	—	-0.90	+0.65	+5.39	—	+5.58	+0.00
	1 ML	$\frac{1}{2}$ -Dissociated	-0.55	-0.60	-0.55 <sup>a</sup>	+1.00 <sup>a</sup>	+4.95	+4.96	+5.27 <sup>a</sup>	-0.31 <sup>a</sup>
$G_0W_0$	$\frac{1}{2}$ ML	Intact	-1.28	—	-1.31	+0.24	+6.17	—	+6.34	+0.76
	1 ML	Intact	-1.88	-1.32	-1.29 <sup>a</sup>	+0.26 <sup>a</sup>	+5.23	+5.29	+5.68 <sup>a</sup>	+0.10 <sup>a</sup>
	$\frac{1}{2}$ ML	Dissociated	-0.65	—	-1.05	+0.50	+6.09	—	+6.04	+0.46
	1 ML	$\frac{1}{2}$ -Dissociated	-1.03	-1.05	-0.97 <sup>a</sup>	+0.57 <sup>a</sup>	+5.42	+5.97	+5.98 <sup>a</sup>	+0.40 <sup>a</sup>
UPS					-1.55 <sup>b</sup>	—				
2PP									+5.58 <sup>c</sup>	—

<sup>a</sup>Ref. 24, <sup>b</sup>Ref. 8, <sup>c</sup>Ref. 11.

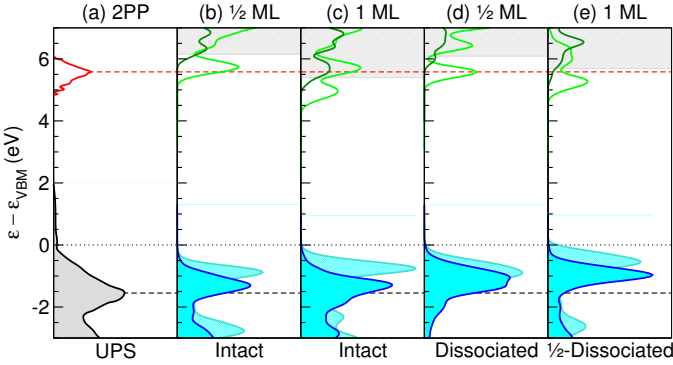


**Fig. 4.**  $\text{CH}_3\text{OH}$  projected (cyan/blue) and Wet (light/dark green) DOS computed with DFT/ $G_0W_0$  for an (b,c) intact, (d) dissociated, and (e)  $\frac{1}{2}$ -dissociated (b,d)  $\frac{1}{2}$  ML and (c,e) 1 ML [24] of  $\text{CH}_3\text{OH}$  on  $\text{TiO}_2(110)$  and the (a) experimental UPS [8] (black) and 2PP spectra [11] (red). Filling denotes occupied levels. Energies are relative to the VBM,  $\varepsilon_{\text{VBM}}$  (black dotted line). Grey shaded regions denote states above the vacuum level  $E_{\text{vac}}$ . Black/red dashed horizontal lines denote the highest/lowest energy peaks in the UPS/2PP spectra.

included in the Wet DOS of Fig. 4.

In Fig. 4 we compare the  $\text{CH}_3\text{OH}$  PDOS and Wet DOS for  $\frac{1}{2}$  ML (intact and dissociated) and 1 ML (intact and  $\frac{1}{2}$ -dissociated) on  $\text{TiO}_2(110)$  with the UPS and 2PP spectra. We focus on the highest energy peak in the UPS, which is at  $\varepsilon_{\text{peak}}^{\text{UPS}} \approx -1.55$  eV relative to the VBM,  $\varepsilon_{\text{VBM}}$  [8]. We find the corresponding peak in the  $\text{CH}_3\text{OH}$  PDOS of both 1 ML and  $\frac{1}{2}$  ML intact structures is in semi-quantitative agreement with the experiment ( $\Delta\varepsilon^{\text{UPS}} \approx 0.25$  eV). The highest energy peak in the  $\text{CH}_3\text{OH}$  PDOS for both  $\frac{1}{2}$  ML dissociated and 1 ML  $\frac{1}{2}$ -dissociated structures is shifted  $\sim 0.54$  eV closer to the VBM compared to the UPS peak. Thus, the  $G_0W_0$  results support the assignment of the UPS highest energy peak to intact  $\text{CH}_3\text{OH}$ , independent of the coverage.

Generally, the energies of the HOMO levels at  $\Gamma$  coincide

with the highest energy PDOS peak. However, the  $\text{CH}_3\text{OH}$  PDOS for the 1 ML intact structure exhibits a pronounced shoulder at  $\sim -1.9$  eV. This feature is directly attributable to the  $\text{HOMO}_D$  at  $-1.88$  eV, while the  $\text{HOMO}_{ND}$  contributes to the main peak at  $-1.29$  eV.

Perhaps more surprising, the  $\text{HOMO}_D$  for the dissociated  $\frac{1}{2}$  ML structure is 0.5 eV above the corresponding PDOS peak. This is observed as a broadening in the PDOS towards higher energies. It is the counterpart of the intact  $\text{HOMO}_D$ , at  $-1.06$  eV, which coincides with the peak energy in the PDOS for the  $\frac{1}{2}$  ML dissociated structure.

To understand this behaviour requires some consideration of the HOMO's energy dispersion and its relation to hybridization with the surface. The more localized a molecular level is, the less its energy dispersion. For the dissociated  $\frac{1}{2}$  ML structure, there is significant hybridization with the  $\text{TiO}_2(110)$  surface. This results in broadening of the HOMO into a band as it mixes with the O  $2p_\pi$  states of the surface.

The 2PP spectrum has an intense experimental peak at  $\varepsilon_{\text{peak}}^{\text{2PP}} \approx 5.58$  eV [11]. As previously reported [24, 25], we find the 2PP spectrum is best reproduced by the 1 ML  $\text{CH}_3\text{OH}$  intact structure ( $\Delta\varepsilon^{\text{2PP}} \sim 0.10$  eV). However, unlike the  $\text{CH}_3\text{OH}$  PDOS peak, we observe a qualitative difference in the Wet DOS with the coverage. In particular, the Wet DOS peak for the  $\frac{1}{2}$  ML intact structure is significantly higher in energy ( $\Delta\varepsilon^{\text{2PP}} \sim 0.76$  eV).

As mentioned above, the 2D  $\text{LUMO}_{\text{Wet}}$  level for the 1 ML  $\frac{1}{2}$ -dissociated structure resembles in energy and spatial distribution the  $\text{LUMO}_{\text{Wet}}$  and  $\text{LUMO}_{\text{Wet}} + 1$  levels for the 1 ML intact structure. Consistent with its 2D character, we find the 2D  $\text{LUMO}_{\text{Wet}}$ 's energy matches the 2PP peak. This suggests there will be  $\text{LUMO}_{\text{Wet}}$  levels with 2D character, which are accessible in the 2PP energy range, even for mixtures of dissociated and intact  $\text{CH}_3\text{OH}$ .

All the  $\text{LUMO}_{\text{Wet}}$  levels contribute to the onset of the Wet DOS with the exception of  $\text{LUMO}_{\text{Wet}} + 1$  for the 1 ML  $\frac{1}{2}$ -dissociated structure. The latter contributes directly to the Wet DOS peak. As we saw for the HOMO levels, hybridization of

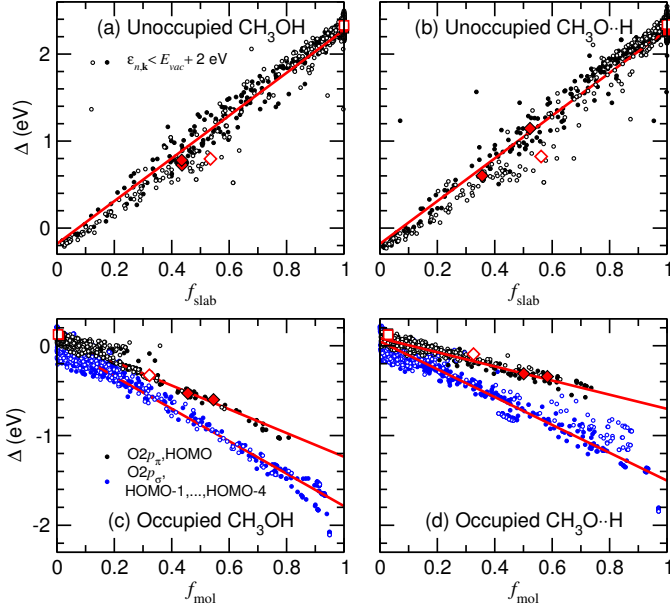


**Fig. 5.**  $G_0W_0$  QP energy correction  $\Delta$  in eV versus fraction of the wavefunction’s density (a,b) in the slab  $f_{\text{slab}}$  for the unoccupied levels and (c,d) in the molecular layer  $f_{\text{mol}}$  for the occupied levels with  $1/2$  ML (open symbols) and 1 ML [24] (filled symbols) of (a,c) intact and (b,d) either dissociated or  $1/2$ -dissociated  $\text{CH}_3\text{OH}$  on  $\text{TiO}_2(110)$ . Diamonds denote the (a,b)  $\text{LUMO}_{\text{Wet}}$ ,  $\text{LUMO}_{\text{Wet}} + 1$ , (c,d)  $\text{HOMO}_D$ ,  $\text{HOMO}_{ND}$  at  $\Gamma$  depicted in Fig. 3. Squares denote the (a,b) CBM and (c,d) VBM levels. Red solid lines are linear fits.

the  $\text{LUMO}_{\text{Wet}}$  levels with the Ti 3d levels results in a broadening of these levels into bands. As a result, we see a distinct broadening of the peaks in the Wet DOS. This broadening is significantly more pronounced for the  $1/2$  ML  $\text{LUMO}_{\text{Wet}}$  levels, due to their stronger hybridization with the surface.

To understand the nature of the observed differences in the QP  $G_0W_0$  corrections to the KS eigenenergies, we consider their relation to the spatial distribution of the KS wavefunction. In Fig. 5 we plot the calculated QP  $G_0W_0$  energy corrections  $\Delta$  versus the fraction of the wavefunction within the surface and molecular layer  $f_{\text{slab}}$  (grey and brown regions in Fig. 3) for the unoccupied levels, and within the molecular layer  $f_{\text{mol}}$  (brown regions in Fig. 3) for the occupied layers. We find the same linear correlations, independent of the  $\text{CH}_3\text{OH}$  coverage, as reported in Refs. 24, 25.

These results suggest that for a molecular level to be available in the 2PP energy regime, it should have little weight in the bulk, i.e., a weak hybridization with the Ti 3d levels. Otherwise, the level would be shifted above the vacuum level. Instead, any accessible level should have significant weight in the vacuum. In effect, any molecular level that meets these criteria could be reasonably classified as a Wet electron level.

Altogether, this suggests these linear correlations may be effectively used to estimate the QP  $G_0W_0$  eigenenergies based on the KS wavefunction’s spatial distribution. This would pave the way for future studies of more complicated  $\text{CH}_3\text{OH}$  over-

layers, and lower coverages, for which  $G_0W_0$  calculations are computationally unfeasible [24].

#### 4. Conclusions

We have performed  $G_0W_0$  calculations for the  $1/2$  ML (intact and dissociated) and 1 ML (intact and  $1/2$ -dissociated)  $\text{CH}_3\text{OH}$  on  $\text{TiO}_2(110)$  structures. These results provide an accurate description of the HOMO/ $\text{LUMO}_{\text{Wet}}$  level alignment on  $\text{TiO}_2(110)$  as a function of the coverage. It is this interfacial level alignment which controls the photocatalytic activity of the system [1, 2, 25].

By comparing our  $G_0W_0$  results to those from standard DFT, we find that the interfacial screening impacts the level alignment qualitatively. This is particularly evident for the  $\text{LUMO}_{\text{Wet}}$  levels of the 1 ML  $1/2$ -dissociated structure, which have different spatial distributions. Although they have the same KS energy, their QP energies are  $\sim 0.55$  eV apart. This is because differences in screening of the wavefunctions are not captured by standard DFT.

We have shown that it is the spatial distribution of the KS wavefunction which determines the QP energy shifts. This is because the wavefunction is screened differently in the three interfacial regions: bulk, molecular, or vacuum. This makes a QP treatment of the anisotropic screening necessary for an interfacial system. In summary, the wavefunction’s spatial distribution controls the QP level alignment.

We find the HOMO wavefunction becomes more hybridized with the substrate as the coverage decreases. As a result, the HOMO energy spans a wide range (1.2 eV) as a function of coverage and dissociation. The HOMO for  $1/2$  ML dissociated  $\text{CH}_3\text{OH}$  on  $\text{TiO}_2$  is the least stable amongst the structures we have considered, at  $-0.65$  eV below the VBM.

This energy suggests that there may exist a nearby nuclear configuration at which a realignment of the energy levels may occur. Further, the strong hybridization of the  $\text{CH}_3\text{O}$  HOMO with the surface O 2p levels suggests a facile hole transfer between these levels. These two points together imply that a hole generated in the  $\text{TiO}_2$  surface via photoexcitation may be transferred to  $\text{CH}_3\text{O}$ . This suggests isolated  $\text{CH}_3\text{O}$  should be a better hole trap than  $\text{CH}_3\text{OH}$ .

Overall, there are two types of  $\text{LUMO}_{\text{Wet}}$  levels: those with 2D character and weight above the surface, and those with a significant hybridization with the surface. At higher coverages, we find a preponderance of 2D  $\text{LUMO}_{\text{Wet}}$  levels, while at lower coverages, the  $\text{LUMO}_{\text{Wet}}$  levels are significantly hybridized with the surface.

The experimentally observed 2PP resonance appears to arise from excitations to 2D  $\text{LUMO}_{\text{Wet}}$  levels. This is contrary to the previous assignment “to the perturbed Ti 3d orbitals caused by the strong interaction of Ti ions with the  $\text{CH}_3\text{O}$  species” [14, 15].

However, one should bear in mind that  $G_0W_0$  tends to over-correct the Ti 3d levels, i.e., the  $\text{TiO}_2$  conduction band minimum (CBM) [25]. This could impact the calculated Wet DOS peak positions for  $\text{LUMO}_{\text{Wet}}$  levels as they are significantly hybridized with the Ti 3d levels.

A correct description of the Ti 3d levels, and hence the CH<sub>3</sub>OH–TiO<sub>2</sub>(110) interface, may require a self-consistent *GW* treatment, including the ionic polarization within the dielectric response function [41]. Finally, one should solve the Bethe-Salpeter Equation (BSE) for a reduced TiO<sub>2</sub>(110) surface to demonstrate whether excitations from reduced Ti<sup>+3</sup> 3d levels to the Wet electron levels have a high oscillator strength [37, 38, 42, 43].

## Acknowledgements

We acknowledge fruitful discussions with Amilcare Iacomino, Jin Zhao, Hrvoje Petek, and Angel Rubio; funding from the Spanish Grants (FIS2012-37549-C05-02, RYC-2011-09582, JCI-2010-08156); and computational time from BSC Red Espanola de Supercomputacion.

## References

- [1] T. L. Thompson, J. T. Yates, Surface science studies of the photoactivation of TiO<sub>2</sub>—new photochemical processes, *Chem. Rev.* 106 (2006) 4428–4453. doi:[10.1021/cr050172k](#).
- [2] M. A. Henderson, A surface science perspective on TiO<sub>2</sub> photocatalysis, *Surf. Sci. Rep.* 66 (2011) 185–297. doi:[10.1016/j.surfrep.2011.01.001](#).
- [3] A. Fujishima, K. Honda, Electrochemical photolysis of water at a semiconductor electrode, *Nature* 238 (1972) 37–38. doi:[10.1038/238037a0](#).
- [4] A. Fujishima, X. Zhang, D. A. Tryk, TiO<sub>2</sub> photocatalysis and related surface phenomena, *Surf. Sci. Rep.* 63 (2008) 515–582. doi:[10.1016/j.surfrep.2008.10.001](#).
- [5] G. M. Whitesides, G. W. Crabtree, Don't forget long-term fundamental research in energy, *Science* 315 (2007) 796–798. doi:[10.1126/science.1140362](#).
- [6] J. Hemminger, G. Crabtree, M. Kastner (Eds.), *The Energy Challenges Report: New Science for a Secure and Sustainable Energy Future*, Argonne National Laboratory, Argonne, Illinois, 2008.
- [7] T. Kawai, T. Sakata, Photocatalytic hydrogen production from liquid methanol and water, *J. Chem. Soc., Chem. Commun.* (1980) 694–695. doi:[10.1039/C39800000694](#).
- [8] H. Onishi, T. Aruga, C. Egawa, Y. Iwasawa, Adsorption of CH<sub>3</sub>OH, HCOOH and SO<sub>2</sub> on TiO<sub>2</sub>(110) and stepped TiO<sub>2</sub>(441) surfaces, *Surf. Sci.* 193 (1988) 33–46. doi:[10.1016/0039-6028\(88\)90321-4](#).
- [9] L.-Q. Wang, K. F. Ferris, J. P. Winokur, A. N. Shultz, D. R. Baer, M. H. Engelhard, Interactions of methanol with stoichiometric and defective TiO<sub>2</sub>(110) and (100) surfaces, *J. Vac. Sci. Tech. A* 16 (1998) 3034–3040. doi:[10.1116/1.581456](#).
- [10] Q. Yuan, Z. Wu, Y. Jin, L. Xu, F. Xiong, Y. Ma, W. Huang, Photocatalytic cross-coupling of methanol and formaldehyde on a rutile TiO<sub>2</sub>(110) surface, *J. Am. Chem. Soc.* 135 (2013) 5212–5219. doi:[10.1021/ja400978r](#).
- [11] K. Onda, B. Li, J. Zhao, H. Petek, The electronic structure of methanol covered TiO<sub>2</sub>(110) surfaces, *Surf. Sci.* 593 (2005) 32–37. doi:[10.1016/j.susc.2005.06.044](#).
- [12] B. Li, J. Zhao, K. Onda, K. D. Jordan, J. Yang, H. Petek, Ultrafast interfacial proton-coupled electron transfer, *Science* 311 (2006) 1436–1440. doi:[10.1126/science.1122190](#).
- [13] K. Onda, B. Li, J. Zhao, K. D. Jordan, J. Yang, H. Petek, Wet electrons at the H<sub>2</sub>O/TiO<sub>2</sub>(110) surface, *Science* 308 (2005) 1154–1158. doi:[10.1126/science.1109366](#).
- [14] C. Zhou, Z. Ren, S. Tan, Z. Ma, X. Mao, D. Dai, H. Fan, X. Yang, J. LaRue, R. Cooper, A. M. Wodtke, Z. Wang, Z. Li, B. Wang, J. Yang, J. Hou, Site-specific photocatalytic splitting of methanol on TiO<sub>2</sub>(110), *Chem. Sci.* 1 (2010) 575–580. doi:[10.1039/C0SC00316F](#).
- [15] C. Zhou, Z. Ma, Z. Ren, A. M. Wodtke, X. Yang, Surface photochemistry probed by two-photon photoemission spectroscopy, *Energy Environ. Sci.* 5 (2012) 6833–6844. doi:[10.1039/c2ee21493h](#).
- [16] M. A. Henderson, I. Lyubinetsky, Molecular-level insights into photocatalysis from scanning probe microscopy studies on TiO<sub>2</sub>(110), *Chem. Rev.* 113 (2013) 4428–4455. doi:[10.1021/cr300315m](#).
- [17] M. Shen, D. P. Acharya, Z. Dohnálek, M. A. Henderson, Importance of diffusion in methanol photochemistry on TiO<sub>2</sub>(110), *J. Phys. Chem. C* 116 (2012) 25465–25469. doi:[10.1021/jp309768b](#).
- [18] M. Shen, M. A. Henderson, Identification of the active species in photochemical hole scavenging reactions of methanol on TiO<sub>2</sub>, *J. Phys. Chem. Lett.* 2 (2011) 2707–2710. doi:[10.1021/jz201242k](#).
- [19] Q. Guo, C. Xu, Z. Ren, W. Yang, Z. Ma, D. Dai, H. Fan, T. K. Minton, X. Yang, Stepwise photocatalytic dissociation of methanol and water on TiO<sub>2</sub>(110), *J. Am. Chem. Soc.* 134 (2012) 13366–13373. doi:[10.1021/ja304049x](#).
- [20] K. R. Phillips, S. C. Jensen, M. Baron, S.-C. Li, C. M. Friend, Sequential photo-oxidation of methanol to methyl formate on TiO<sub>2</sub>(110), *J. Am. Chem. Soc.* 135 (2013) 574–577. doi:[10.1021/ja3106797](#).
- [21] C. Xu, W. Yang, Z. Ren, D. Dai, Q. Guo, T. K. Minton, X. Yang, Strong photon energy dependence of the photocatalytic dissociation rate of methanol on TiO<sub>2</sub>(110), *J. Am. Chem. Soc.* 135 (2013) 19039–19045. doi:[10.1021/ja4114598](#).
- [22] C. Xu, W. Yang, Q. Guo, D. Dai, M. Chen, X. Yang, Molecular hydrogen formation from photocatalysis of methanol on TiO<sub>2</sub>(110), *J. Am. Chem. Soc.* 135 (2013) 10206–10209. doi:[10.1021/ja4030963](#).
- [23] S. Tan, H. Feng, Y. Ji, Y. Wang, J. Zhao, A. Zhao, B. Wang, Y. Luo, J. Yang, J. G. Hou, Observation of photocatalytic dissociation of water on terminal ti sites of tio2(110)-1 1 surface, *Journal of the American Chemical Society* 134 (2012) 9978–9985. doi:[10.1021/ja211919k](#).
- [24] A. Migani, D. J. Mowbray, A. Iacomino, J. Zhao, H. Petek, A. Rubio, Level alignment of a prototypical photocatalytic system: Methanol on TiO<sub>2</sub>(110), *J. Am. Chem. Soc.* 135 (2013) 11429–11432. doi:[10.1021/ja4036994](#).
- [25] A. Migani, D. J. Mowbray, J. Zhao, H. Petek, A. Rubio, Quasiparticle level alignment for photocatalytic interfaces, *J. Chem. Theor. Comp.* (2014). doi:[10.1021/ct500087v](#).
- [26] J. Zhao, J. Yang, H. Petek, Theoretical study of the molecular and electronic structure of methanol on a TiO<sub>2</sub>(110) surface, *Phys. Rev. B* 80 (2009) 235416. doi:[10.1103/PhysRevB.80.235416](#).
- [27] C. E. Patrick, F. Giustino, Quantitative analysis of valence photoemission spectra and quasiparticle excitations at chromophore-semiconductor interfaces, *Phys. Rev. Lett.* 109 (2012) 116801. doi:[10.1103/PhysRevLett.109.116801](#).
- [28] C. Freysoldt, P. Rinke, M. Scheffler, Controlling polarization at insulating surfaces: Quasiparticle calculations for molecules adsorbed on insulator films, *Phys. Rev. Lett.* 103 (2009) 056803. doi:[10.1103/PhysRevLett.103.056803](#).
- [29] J. B. Neaton, M. S. Hybertsen, S. G. Louie, Renormalization of molecular electronic levels at metal-molecule interfaces, *Phys. Rev. Lett.* 97 (2006) 216405. doi:[10.1103/PhysRevLett.97.216405](#).
- [30] J. M. Garcia-Lastra, C. Rostgaard, A. Rubio, K. S. Thygesen, Polarization-induced renormalization of molecular levels at metallic and semiconducting surfaces, *Phys. Rev. B* 80 (2009) 245427. doi:[10.1103/PhysRevB.80.245427](#).
- [31] L. Hedin, New method for calculating the one-particle Green's function with application to the electron-gas problem, *Phys. Rev.* 139 (1965) A796–A823. doi:[10.1103/PhysRev.139.A796](#).
- [32] G. Onida, L. Reining, A. Rubio, Electronic excitations: density-functional versus many-body Green's-function approaches, *Rev. Mod. Phys.* 74 (2002) 601–659. doi:[10.1103/RevModPhys.74.601](#).
- [33] M. Shishkin, G. Kresse, Implementation and performance of the frequency-dependent *GW* method within the PAW framework, *Phys. Rev. B* 74 (2006) 035101. doi:[10.1103/PhysRevB.74.035101](#).
- [34] G. Kresse, D. Joubert, From ultrasoft pseudopotentials to the projector augmented-wave method, *Phys. Rev. B* 59 (1999) 1758. doi:[10.1103/PhysRevB.59.1758](#).
- [35] J. P. Perdew, K. Burke, M. Ernzerhof, Generalized gradient approximation made simple, *Phys. Rev. Lett.* 77 (1996) 3865. doi:[10.1103/PhysRevLett.77.3865](#).
- [36] G. Kresse, J. Furthmüller, Efficient iterative schemes for ab initio total-energy calculations using a plane-wave basis set, *Phys. Rev. B* 54 (1996) 11169. doi:[10.1103/PhysRevB.54.11169](#).
- [37] W. Kang, M. S. Hybertsen, Quasiparticle and optical properties of ru-

- tile and anatase  $\text{TiO}_2$ , Phys. Rev. B 82 (2010) 085203. doi:[10.1103/PhysRevB.82.085203](https://doi.org/10.1103/PhysRevB.82.085203).
- [38] L. Chiodo, J. M. García-Lastra, A. Iacomino, S. Ossicini, J. Zhao, H. Pekt, A. Rubio, Self-energy and excitonic effects in the electronic and optical properties of  $\text{TiO}_2$  crystalline phases, Phys. Rev. B 82 (2010) 045207. doi:[10.1103/PhysRevB.82.045207](https://doi.org/10.1103/PhysRevB.82.045207).
- [39] J. K. Burdett, T. Hughbanks, G. J. Miller, J. W. Richardson, J. V. Smith, Structural-electronic relationships in inorganic solids: powder neutron diffraction studies of the rutile and anatase polymorphs of titanium dioxide at 15 and 295 K, J. Am. Chem. Soc. 109 (1987) 3639–3646. doi:[10.1021/ja00246a021](https://doi.org/10.1021/ja00246a021).
- [40] D. J. Mowbray, J. I. Martínez, F. Calle-Vallejo, J. Rossmeisl, K. S. Thygesen, K. W. Jacobsen, J. K. Nørskov, Trends in metal oxide stability for nanorods, nanotubes, and surfaces, J. Phys. Chem. C 115 (2011) 2244–2252. doi:[10.1021/jp110489u](https://doi.org/10.1021/jp110489u).
- [41] M. A. L. Marques, J. Vidal, M. J. T. Oliveira, L. Reining, S. Botti, Density-based mixing parameter for hybrid functionals, Phys. Rev. B 83 (2011) 035119. doi:[10.1103/PhysRevB.83.035119](https://doi.org/10.1103/PhysRevB.83.035119).
- [42] J. M. Garcia-Lastra, K. S. Thygesen, Renormalization of optical excitations in molecules near a metal surface, Phys. Rev. Lett. 106 (2011) 187402. doi:[10.1103/PhysRevLett.106.187402](https://doi.org/10.1103/PhysRevLett.106.187402).
- [43] V. Despoja, I. Lončarić, D. J. Mowbray, L. Marušić, Quasiparticle spectra and excitons of organic molecules deposited on substrates:  $G_0W_0$ -BSE approach applied to benzene on graphene and metallic substrates, Phys. Rev. B 88 (2013) 235437. doi:[10.1103/PhysRevB.88.235437](https://doi.org/10.1103/PhysRevB.88.235437).